The Astrophysical Journal, 832:64 (9pp), 2016 November 20 doi:10.3847/0004-637X/832/1/64

MIXING THE SOLAR WIND PROTON AND ELECTRON SCALES: EFFECTS OF ELECTRON TEMPERATURE ANISOTROPY ON THE OBLIQUE PROTON FIREHOSE INSTABILITY

Y. Maneva[1], M. Lazar[1,2,3], A. Viñas[4], and S. Poedts[1]
[1] Centre for Mathematical Plasma Astrophysics, Celestijnenlaan 200B, 3001 Heverlee, Belgium; yana.maneva@wis.kuleuven.be
[2] Royal Belgian Institute for Space Aeronomy 3-Avenue Circulaire, B-1180 Brussels, Belgium
[3] Institut für Theoretische Physik, Lehrstuhl IV: Weltraum- und Astrophysik, Ruhr-Universität Bochum, D-44780 Bochum, Germany
[4] NASA Goddard Space Flight Center, Heliophysics Science Division, Greenbelt, MD 20771, USA
Received 2016 March 14; revised 2016 September 14; accepted 2016 September 16; published 2016 November 17

ABSTRACT

The double adiabatic expansion of the nearly collisionless solar wind plasma creates conditions for the firehose instability to develop and efficiently prevent the further increase of the plasma temperature in the direction parallel to the interplanetary magnetic field. The conditions imposed by the firehose instability have been extensively studied using idealized approaches that ignore the mutual effects of electrons and protons. Recently, more realistic approaches have been proposed that take into account the interplay between electrons and protons, unveiling new regimes of the parallel oscillatory modes. However, for oblique wave propagation the instability develops distinct branches that grow much faster and may therefore be more efficient than the parallel firehose instability in constraining the temperature anisotropy of the plasma particles. This paper reports for the first time on the effects of electron plasma properties on the oblique proton firehose (PFH) instability and provides a comprehensive vision of the entire unstable wave-vector spectrum, unifying the proton and the smaller electron scales. The plasma β and temperature anisotropy regimes considered here are specific for the solar wind and magnetospheric conditions, and enable the electrons and protons to interact via the excited electromagnetic fluctuations. For the selected parameters, simultaneous electron and PFH instabilities can be observed with a dispersion spectrum of the electron firehose (EFH) extending toward the proton scales. Growth rates of the PFH instability are markedly boosted by the anisotropic electrons, especially in the oblique direction where the EFH growth rates are orders of magnitude higher.

Key words: instabilities – plasmas – solar wind – waves

1. INTRODUCTION

In the hot and dilute space plasmas where particle collisions are poor and inefficient for plasma scattering, the enhanced electromagnetic fluctuations and subsequent wave-particle interactions should play the major role in triggering the transport of energy and momentum. The properties of the electromagnetic fluctuations at kinetic ion (proton) and electron scales are continuously reported by observations in the solar wind and planetary magnetospheres (Zimbardo et al. 2010; Bruno & Carbone 2013), and yet their origin is not fully understood. Some of the observed fluctuations originate in the large-scale perturbations produced by the coronal outflows in the solar atmosphere, which are then transported by the super-Alfvénic solar wind and undergo a large-scale decay to smaller scales where their dissipation occurs. Another part of the fluctuations observed at small proton and electron scales can be generated locally by the kinetic instabilities which are driven by non-thermal features in the particle velocity distributions, such as temperature anisotropy, particle beams and differential streaming (Nguyen et al. 2007; Bale et al. 2009; Jian et al. 2009; Kasper et al. 2013; Maneva et al. 2015a, 2015b).

At present, the double-adiabatic descriptions are limited and do not take into account electron or ion heat flux corrections. In principle, in the presence of large parallel temperatures, a heat flux term needs to be added to the double-adiabatic equation, which could prevent the parallel temperature from further growth. Without the heat flux corrections, the double-adiabatic theory predicts an indefinite increase of the parallel temperature component in the direction of the interplanetary magnetic field. One way to reduce this indefinite growth is through fluid and kinetic plasma instabilities. Among the kinetic instabilities, the firehose instability is believed to be sufficiently efficient to prevent the indefinite increase of the plasma temperature along the interplanetary magnetic field, as predicted by the double adiabatic expansion of the solar wind plasma (Hellinger & Matsumoto 2000; Gary & Nishimura 2003; Camporeale & Burgess 2008; Hellinger et al. 2014; Yoon & Seough 2014). If the temperature anisotropy exceeds the instability thresholds, firehose modes are destabilized and the excited fluctuations may react back on plasma particles, reducing their anisotropy. Susceptible to the firehose instability are both the electron and proton species. Thus, whenever the parallel component of the electron temperature significantly exceeds the perpendicular one, the electron temperature anisotropy results in the electron firehose (EFH) instability. Similarly above the threshold value, the proton temperature anisotropy can trigger proton firehose (PFH) instability. Each of these two instabilities may destabilize two branches of electromagnetic modes, oscillatory or periodic waves with a finite wave-frequency $\Re(\omega) \neq 0$ in parallel and quasi-parallel direction, and aperiodic modes with $\Re(\omega) = 0$ propagating obliquely to the magnetic field. The quasi-parallel waves have characteristic frequencies and growth rates in the range of the proton cyclotron frequency and below, such that the EFH modes, which are left-handed (LH) circularly polarized, can interact resonantly with the protons, see Paesold & Benz (1999), Messmer (2002) and the references therein. On the other hand, the electrons may have an impact on PFH instability by changing the phase velocity of the excited fluctuations, which may subsequently increase the number of resonant protons and, implicitly, enhance the growth rate of the instability (Kennel &

Scarf 1968). Despite the indications of a potential interplay between electrons and protons, the EFH and PFH instabilities are studied separately on the basis of simplified (idealized) models which ignore the mutual effects of electrons and protons (Hellinger & Matsumoto 2000; Li & Habbal 2000; Gary & Nishimura 2003; Hellinger et al. 2006; Camporeale & Burgess 2008; Lazar & Poedts 2009; Viñas et al. 2015).

Recently, more realistic advanced approaches have been proposed to investigate the effects of temperature anisotropy driven instabilities in space plasmas, by considering the interplay of the anisotropic electrons and anisotropic protons (Michno et al. 2014; Navarro et al. 2014; Shaaban et al. 2015; Viñas et al. 2015). Thus, mutual effects of electrons and ions have already been studied for conditions favorable to the PFH instability (Kennel & Scarf 1968; Lazar et al. 2011; Michno et al. 2014), and the electromagnetic ion (proton) cyclotron instability (Shaaban et al. 2015), but only for modes propagating in directions parallel to the magnetic field. In directions oblique to the magnetic field, both the EFH and PFH instabilities exhibit distinct aperiodic branches, which develop much faster than the parallel PFH (Li & Habbal 2000; Hellinger & Matsumoto 2000; Camporeale & Burgess 2008) and may therefore be more efficient in the relaxation process. We should note that for isotropic electrons the growth rate of the aperiodic PFH instability is much lower than that of the periodic branch.

In this paper, we present the results from linear instability study which demonstrates the interplay of the oblique PFH and EFH branches under the mutual effects of electron and proton temperature anisotropies. The oblique branches are described together with the quasi-parallel modes, enabling us to compare them and check under which circumstances the aperiodic instability remains faster, i.e., with higher growth rates than the periodic one. We investigate the effects of electron properties, such as plasma β and temperature anisotropy, on the frequency and the growth rate of the PFH instability. Our linear dispersion instability analysis is based on a kinetic Vlasov–Maxwell formalism for a non-drifting anisotropic electron–proton plasma. The details of this kinetic formalism are given in Section 2. The intrinsically oblique dispersion solver is capable of describing electromagnetic modes propagating at an arbitrary angle with respect to the magnetic field (the angle between the wave-vector of the excited fluctuations and the background magnetic field). In Section 3 we present the unstable solutions for hot and highly anisotropic components in high-β regimes relevant for the solar wind plasma conditions reported by different spacecraft. The instability analysis is performed for a wide range of wave-vectors coupling the proton and the smaller electron scales. We provide the frequency and propagation angle dependence of the unstable wave-vector spectrum, which enables us to study both the oblique and quasi-parallel branches, and check whether their distinct features, namely the aperiodicity and oscillatory nature, remain the same under the cumulative influence of electrons and protons. In Section 4 we summarize our results and discuss the implications of the electron–proton scale mixing for the effects of the EFH and PFH instabilities in solar wind and space plasmas.

2. LINEAR DISPERSION ANALYSIS FOR AN ARBITRARY ANGLE OF PROPAGATION. PLADAWAN SOLVER

In this section, we present the basis of the kinetic dispersion solver, used to find the specific properties of the linear electromagnetic waves generated in a hot non-relativistic firehose-unstable plasma with anisotropic electrons and protons. We assume a homogeneous magnetized plasma with gyrotropic distributions of electrons ($s = e$) and protons ($s = p$), which are well described by non-drifting bi-Maxwellian distribution functions:

$$f_s(v_\parallel, v_\perp) = \frac{1}{\pi^{3/2}\alpha_{\parallel,s}\alpha_{\perp,s}^2}\exp\left(-\frac{v_\parallel^2}{\alpha_{\parallel,s}^2} - \frac{v_\perp^2}{\alpha_{\perp,s}^2}\right) \quad (1)$$

normalized to unity. In this model, $\alpha_{\perp,\parallel s} = (2k_B T_{\perp,\parallel s}/m_s)$ represent the thermal velocities in directions perpendicular and parallel to the background magnetic field, and $\mu_s = \alpha_{\perp s}^2/\alpha_{\parallel s}^2 = T_\perp/T_\parallel$ is the temperature anisotropy of particle species s.

If we assume an equilibrium state which satisfies charge neutrality and current conservation, the general dispersion relation for warm plasma modes propagating at an arbitrary angle with respect to a uniform magnetic field $\boldsymbol{B} = B_0\hat{z}$ is given by (Stix 1962; Montgomery & Tidman 1964; Ichimaru 1973; Krall & Trivelpiece 1973; Viñas et al. 2000)

$$0 = \det D(\omega, k, \theta) \quad (2)$$

with

$$D(\omega, k, \theta) = \begin{vmatrix} 1 - \frac{k_\parallel^2 c^2}{\omega^2} + Q_{xx} & Q_{xy} & \frac{k_\parallel k_\perp c^2}{\omega^2} + Q_{xz} \\ Q_{yx} & 1 - \frac{k^2 c^2}{\omega^2} + Q_{yy} & Q_{yz} \\ \frac{k_\parallel k_\perp c^2}{\omega^2} + Q_{zx} & Q_{zy} & 1 - \frac{k_\perp^2 c^2}{\omega^2} + Q_{zz} \end{vmatrix}.$$

The different elements of the susceptibility tensor can be expressed in terms of the Fried-Conte plasma dispersion function $Z(\xi_s)$ and the modified Bessel functions $I_n(\lambda_s)$ as follows

$$\begin{aligned}
Q_{xx} &= 2\sum_s \sum_{n=-\infty}^{n=+\infty} \frac{\omega_{ps}^2}{\omega^2}\Lambda_n \frac{n^2\Omega_s^2}{k_\perp^2\alpha_{\perp s}^2}[\mu_s - 1 + \mu_s\bar{\xi}_s Z(\xi_s)], \\
Q_{xy} &= -Q_{yx} = 2i\sum_s \sum_{n=-\infty}^{n=+\infty} \frac{\omega_{ps}^2}{\omega^2}\left(\frac{n\Lambda_n'}{2}\right)\mu_s\bar{\xi}_s Z(\xi_s), \\
Q_{xz} &= Q_{zx} = 2\sum_s \sum_{n=-\infty}^{n=+\infty} \frac{\omega_{ps}^2}{\omega^2}\Lambda_n \frac{n\Omega_s}{k_\perp\alpha_{\perp s}} \\
&\quad \times [(\mu_s^{-1} - 1)\frac{n\Omega_s}{k_\parallel\alpha_{\parallel s}} + \xi_s\bar{\xi}_s Z(\xi_s)], \\
Q_{yy} &= 2\sum_s \sum_{n=-\infty}^{n=+\infty} \frac{\omega_{ps}^2}{\omega^2}\frac{\Omega_s^2}{k_\perp^2\alpha_{\perp s}^2}(n^2\Lambda_n - 2\lambda_s^2\Lambda_n') \\
&\quad \times [\mu_s - 1 + \mu_s\bar{\xi}_s Z(\xi_s)], \\
Q_{yz} &= -Q_{zy} = -2i\sum_s \sum_{n=-\infty}^{n=+\infty} \frac{\omega_{ps}^2}{\omega^2}\frac{\Omega_s}{k_\perp\alpha_{\parallel s}}\lambda_s\Lambda_n' \\
&\quad \times \xi_s\bar{\xi}_s Z(\xi_s), \\
Q_{zz} &= 2\sum_s \sum_{n=-\infty}^{n=+\infty} \frac{\omega_{ps}^2}{\omega^2}\Lambda_n \\
&\quad \times \left[\frac{\omega^2}{k_\parallel^2\alpha_{\parallel s}^2} + (1 - \mu_s^{-1})\frac{n^2\Omega_s^2}{k_\parallel^2\alpha_{\parallel s}^2} + \xi_s^2\bar{\xi}_s Z(\xi_s)\right]. \quad (3)
\end{aligned}$$

In the expressions above, we have used the standard definition for the plasma dispersion function $Z(\xi_s)$

$$Z(\xi_s) = \frac{1}{\sqrt{\pi}} \int_{-\infty}^{\infty} \frac{\exp(-t^2)}{t - \xi_s} dt. \quad (4)$$

$\Lambda_n(\lambda_s)$ is related to the modified Bessels function of the first kind $I_n(\lambda_s)$

$$\Lambda_n(\lambda_s) = I_n(\lambda_s)\exp(-\lambda_s), \quad (5)$$

and the arguments of the special functions can be expressed as

$$\xi_s = \frac{\omega - n\Omega_s}{k_\parallel \alpha_{\parallel s}}, \quad \bar{\xi}_s = \frac{\omega - n\Omega_s(1 - \mu_s^{-1})}{k_\parallel \alpha_{\parallel s}}, \quad \lambda_s = \frac{k_\perp^2 \alpha_{\perp s}^2}{2\Omega_s^2}. \quad (6)$$

To find the plasma dispersion relations and perform the spectral analysis, in this paper we have used a linear Vlasov instability dispersion solver, called PLADAWAN, which stands for Plasma Dispersion and Wave Analyzer. The entire code has been written in IDL by A.F. Viñas, with the assistance of many former postdoctoral researchers and collaborators. Although not presented in this paper, PLADAWAN provides an opportunity to diagnose additional dispersion properties, such as polarization, helicity, etc. The root-finder in the code is based on the IDL Müller-method solver for arbitrary complex functions. The values of the Fried-Conte plasma dispersion function $Z(\xi)$ (Fried & Conte 1961) in the code are determined via a Pade approximant with 15 coefficients. In general, the code can be used to calculate the dispersion relation in a differentially streaming multi-component multi-species anisotropic plasma. For the purpose of this study, we will consider the simple case of non-drifting anisotropic electron–proton plasma, where the electrons and ions are treated as single species without taking into account beam components, nor the electron strahl. Adding differential streaming between the protons and the electrons modifies the dispersion relation and results in additional fast growing modes, which will not be considered here.

3. RESULTS

In this section we apply the linear Vlasov–Maxwell dispersion formalism described above and employ PLADAWAN to find solutions in the case of non-drifting non-relativistic quasi-neutral plasma, consisting of anisotropic electrons and protons. All units in this study have been normalized to the proton cyclotron frequency and the ion-inertial length, d_i based upon the proton density and the proton mass. The true electron-to-proton mass ratio has been used and different values of the plasma $\beta_\parallel$ have been considered, where, by definition, $\beta_{\parallel e,p} = 8\pi n_{e,p} T_{\parallel e,p}/B_0^2$, and the charge neutrality of the equilibrium background state ensures that $n_e = n_p$. Assuming conditions favorable to both the PFH and EFH instabilities, this section presents the results of a linear instability study for an extended range of propagation angles, i.e., from a direction parallel to the background magnetic field to highly oblique angles approaching perpendicular wave propagation. A detailed characterization of the interplay of these two instabilities is proposed first, covering both their periodic and aperiodic branches. Later on, we focus on the PFH instability and describe the effects of anisotropic electrons on the PFH instability.

3.1. Interplay of PFH and EFH Instabilities

Our analysis starts with the case of simultaneously anisotropic protons and electrons that matches the early test case of the mixed parallel PFH and EFH instabilities (with two distinct peaks at the proton scales) as considered in Michno et al. (2014). The plasma parameters for this case study are given by $(T_\perp/T_\parallel)_p = 0.4$, $(T_\perp/T_\parallel)_e = 0.5$,$\beta_{p\parallel} = 3.0$, $\beta_{e\parallel} = 4.0$. We have solved the general dispersion relation, see Equation (2) in Section 2, to simultaneously follow the evolution of the PFH and the EFH instabilities at different angles of propagation. For this case, the unstable solutions may be characterized by the generic examples displayed in Figures 1 and 2, which show a dispersion highly dependent on both the magnitude and orientation of the wave-vector k. Since there are no drifts in the system, the solutions are symmetric with respect to the wave-vector direction as given by the (positive or negative) sign of k, such that we can consider only solutions with $k > 0$, enabling us to identify the unstable solutions with $\Im(\omega) > 0$, and among the periodic modes with $\Re(\omega) \neq 0$ to distinguish those with different polarizations. The periodic PFH (PPFH) modes are right-hand (RH) polarized with $\Re(\omega) > 0$ while the periodic EFH (PEFH) modes are left-hand (LH) polarized with $\Re(\omega) < 0$. To distinguish between the RH-polarized PPFH and LH-polarized PEFH modes in Figures 1 and 2 on top of the real frequencies and the growth rates we have over-plotted the zero-frequency line, which marks the transition from RH to LH polarization. The definition of the polarization $\mathcal{P}$ used throughout this paper is the standard definition in the plasma frame, $\mathcal{P} = i(E_x/E_y)\mathrm{sign}(\omega)$, see for example, (Baumjohann & Treumann 1996). The components of the fluctuating electric field are calculated through the dispersion relation and the polarization depends on the magnetic helicity and the direction of propagation. For RH circularly polarized waves such as PPFH and fast magnetosonic modes $\mathcal{P} = 1$ and for left-hand circularly polarized waves, such as PEFH and Alfvén/ion-cyclotron modes the polarization is $\mathcal{P} = -1$. We should note that the polarization of the propagating firehose-unstable modes is strictly circular only for the case of parallel wave propagation. More generally, the periodic oblique firehose branches are elliptically polarized. The non-propagating aperiodic modes are linearly polarized. For the case of aperiodic instabilities, the zero-growth rate line has been added to better identify the onset of the instabilities.

Each panel of Figure 1 describes the wave-number dispersion of the growth rate (green lines) and the wave frequency (red lines) for a certain angle of propagation. In a parallel direction, at exactly 0°, the firehose solutions become unstable only at low wave-numbers at the proton scales. The top panel of Figure 1 shows two peaks of periodic modes, namely, the RH PPFH and the LH PEFH. For a small angle of propagation of only 5°, these two peaks of periodic modes are still present, but between them we can already observe a third peak arising, and this peak may be associated with an aperiodic EFH (AEFH) instability. The aperiodic (or non-propagating) modes are characterized by $\Re(\omega) = 0$, and the APFH and AEFH peaks in Figures 1 and 2 clearly satisfy this condition. Li & Habbal (2000) have assumed isotropic protons, and showed that with increasing angle of propagation the AEFH modes arise at low wave-numbers, while the PEFH instabilities are restrained to higher wave-numbers. In our study, the protons are considered anisotropic, therefore the dominant instability at low wave-numbers and small propagation angles is the PFH.

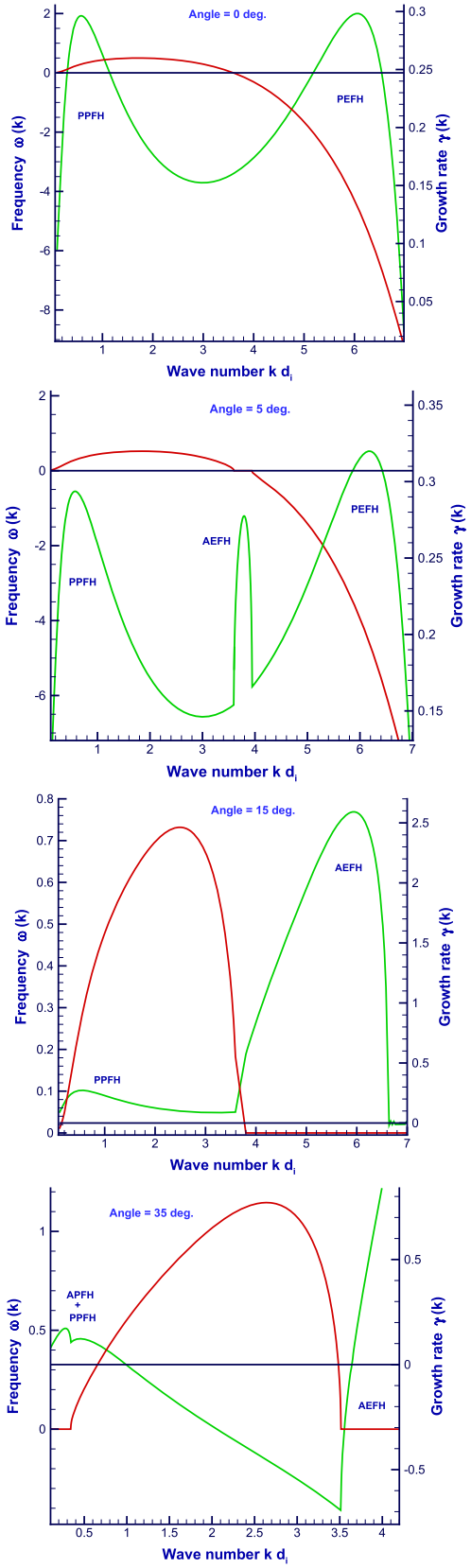

Figure 1. Frequency (red) and growth rate (green) dispersion relations at small wave-numbers for propagation angles 0° (top), 5°, 15°, and 35°. Plasma parameters: $(T_\perp/T_\parallel)_p = 0.4$, $(T_\perp/T_\parallel)_e = 0.5$, $\beta_{p\parallel} = 3.0$, $\beta_{e\parallel} = 4.0$. The instability peaks such as PPFH, APFH, PEFH, and AEFH are explained in the text.

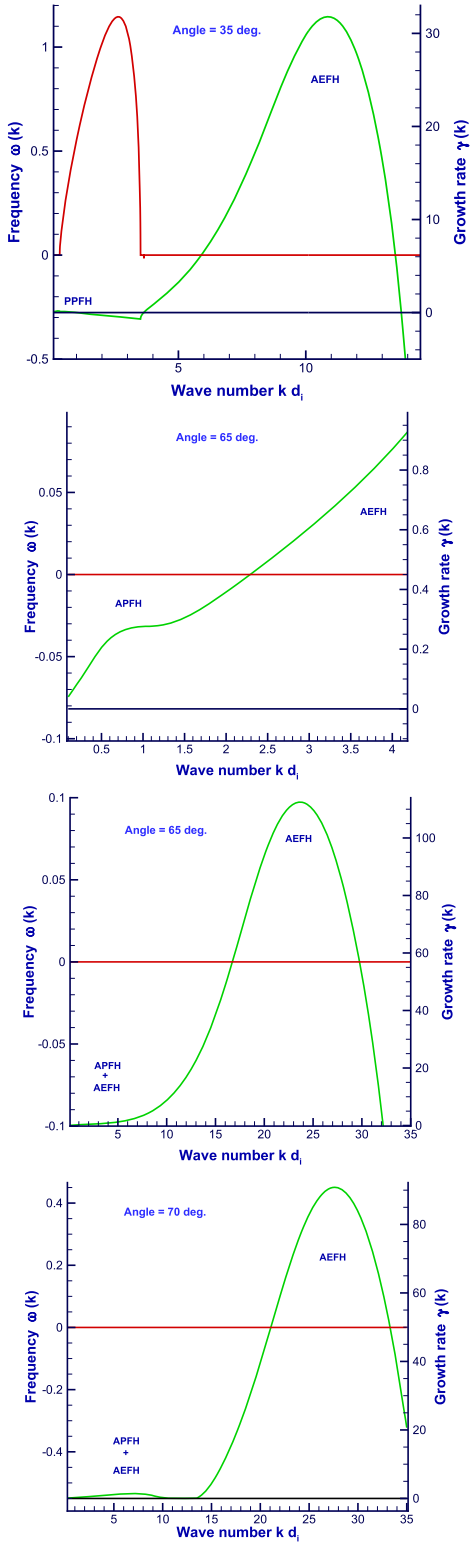

Figure 2. Dispersion relation with the real frequency (red) and growth-rate (green) at various wave-numbers and propagation angles. The figure illustrates the small scales extension of the PPFH mode with a transition to AEFH mode at 35° (top), as well as the evolution of the APFH and AEFH peaks at 65° and 70°.

For parallel wave propagation, the PPFH and PEFH instabilities occur at similar spatial and temporal scales. However, as we increase the angle of propagation, the growth

rate of the EFH instabilities quickly exceeds the growth rate of the PFH. Simultaneously, the periodic instabilities are quickly getting restrained and eventually do not develop at all. Already at 10° the EFH instability becomes fully aperiodic and the AEFH instability remains dominant throughout the rest of the propagation angles. At 15° the AEFH instability develops much quicker than the PPFH and its growth rate becomes more than an order of magnitude higher. At 35°, we observe the onset of APFH instability at large scales, which grows faster than, and overtakes, the PPFH one. Simultaneously, the growth rate of the AEFH continues to increase and its peak gradually shifts toward larger wave-numbers with increasing angle of propagation, see also Figure 2. The small-scales extension of the AEFH instability at 35°, as well as the evolution of the PFH and the EFH instabilities at higher propagation angles are shown in Figure 2. Above 35° the PPFH mode is fully dominated by the APFH and the AEFH modes, which begin to overlap at the proton scales. The evolution of the APFH branch at large scales, for the highly oblique angle of 65°, is presented on the second panel from top on Figure 2. This angle marks the maximum growth rate for the EFH instability plotted here, which is purely aperiodic. The peak of this AEFH branch develops at approximately $22kd_i$. For propagation at higher angles, the growth rate of the AEFH instability decreases, as seen for the case of 70° in the bottom panel of the figure. At 65° and 70° the AEFH peak is approximately two orders of magnitude higher than the APFH peak. Nevertheless, the APFH peak remains visible at large scales and couples to the AEFH instability there. The peaks marked by AEFH + APFH may be explained as a cumulative effect resulting from the interplay of these two aperiodic instabilities at the intermediary scales.

Although not shown here, at 75° the growth rate of the AEFH decreases by almost two orders of magnitude from approximately $90\Omega_p$ at 70° to approximately $1.2\Omega_p$. At 80° and above the growth rate of the AEFH continues to decrease to $\gamma(k) < 0.5\Omega_p$ and the instability extends down to the very large protons scales, co-existing with the APFH branch even when a strictly perpendicular angle of propagation is reached.

In order to compare the instability peaks and further elaborate on the interplay of the PFH and the EFH instabilities, we choose to display the unstable solutions within the same plot at various selected propagation angles. Figure 3 displays the unstable solutions at large scales (low wave-numbers), where both the periodic and aperiodic modes can be present, depending on the propagation angle. The real frequency of the periodic oscillations in Figure 3 is plotted in red and the growth rates for various propagation angles are represented by different colors as indicated by the labels. For representation purposes, from the complete angular spectrum we have limited the plot to a discrete number of directions that are most relevant for our analysis. The figure is focused on the angular dependence of the instabilities at the proton scales until $kd_i = 4$. The real frequency is plotted for $\theta = 0°$, 15°, 20°, and 30°. Above 35° the PFH becomes strictly aperiodic and there are no growing propagating solutions related to the PFH nor to the EFH instabilities at all scales. The growth rates for the oscillatory PPFH branches for $\theta = 0°$, 15°, 20°, and 30°, as well as the growth rates for the non-propagating APFH modes at $\theta = 40°$, 45°, 50°, 60°, and 85° are over-plotted with various colors. For wave-numbers $kd_i > 4$, only the aperiodic firehose solutions for both protons and electrons have positive growth rates, and

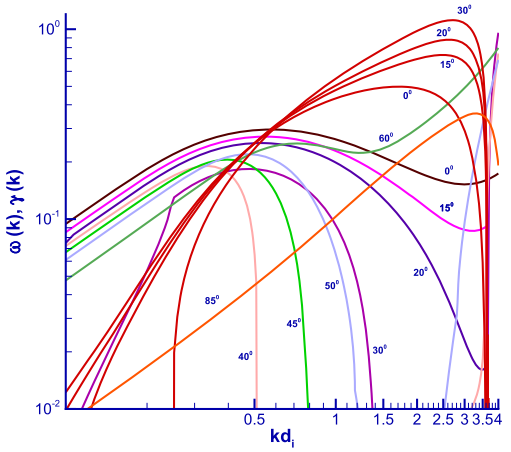

Figure 3. Low wave-number dispersion (proton scales) of the wave frequency (red lines) and growth rates (various color lines) for different angles of propagation (see labels). Units are normalized to the proton inertial length d_i and the proton gyro-frequency Ω_p, and the plasma parameters are the same as in Figure 1.

these are shown in the next Figure 4. At smaller proton and electron scales the PPFH branches are fully damped and remain stable at all propagation angles.

The top panel of Figure 4 shows the dependence of the PFH and EFH instability growth rates at various angles from large to small scales. The bottom panel shows only the AEFH instabilities for $kd_i \geqslant 4$ and $\theta \geqslant 10°$. To generate the angular dependence we have varied the propagation angle with steps of 5° within a wave-number interval of $kd_i = [0.05, 35]$. We have chosen 1000 points in wave-number space at each propagation angle and have selected the fastest growing solution. The growth rates on the top panel show distinct double peak structures corresponding to the PFH and the EFH instabilities. The periodic modes are specific to the large proton scales approximately until $kd_i = 3.5$. The PFH instabilities are propagating (PPFH) until $\theta \leqslant 35°$, after which the growing solutions at large scales are dominated by the APFH branches. The PEFH solutions are visible until $\theta < 10°$, above which they become quickly overcome by the AEFH branches. The unstable wave-number range of the PPFH instabilities shrinks with increasing angle of propagation, as the transition from periodic to aperiodic modes occur. Simultaneously, the unstable range for the AEFH instability increases. For highly oblique angles $\theta > 60°$ the unstable modes become purely aperiodic, and the growth rates may exhibit multiple peaks corresponding to the aperiodic APFH and AEFH instabilities. For better data representation of the growth rate and to avoid the effects of mode-mixing between the PFH and the EFH modes, in the bottom panel we have restricted the scales for wave-numbers $k \geqslant 4d_i^{-1}$ and have imposed a limit on the minimum growth rate for the plot, $\gamma > 1.5\Omega_p$, thus omitting the slowly growing quasi-parallel PEFH modes at $\theta < 10°$. Initially, the AEFH peak is more than one order of magnitude higher than the APFH peak, and this difference increases with the angle of propagation exceeding two order of magnitude. For the case parameters studied here, the AEFH peak shows a maximum growth rate of $\gamma > 100\Omega_p$ at about 63°, see the bottom panel of Figure 4. The periodic branches of the EFH and PFH instabilities are clearly described at small angles in Figure 1, as well as in Figure 3.

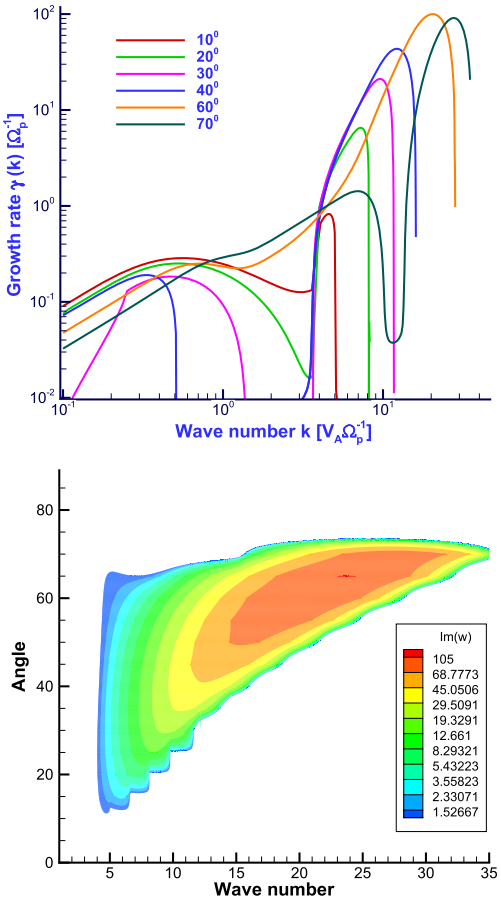

Figure 4. Top panel: the PHF and EFH instability growth rates as a function of wave-number k and propagation angle θ for an extended wavelength range including the electron scales. Bottom panel: 3D representation of the EFH instability as a function of k and θ. Normalizations and plasma parameters are the same as in Figure 3.

As noted above the wave-number, variation of the growth rate with increasing propagation angles is not monotonous, and may show an additional intermediary peak. This peak appears to be a reminiscence from the interplay of the PFH and EFH instabilities, which determines the maximum growth rate of APFH branch to be shifted toward the smaller electron scales. The shift of the maximum growth rate toward shorter wavelengths at higher angles of propagation is similar to the one observed by Li & Habbal (2000) for the case of pure EFH instability with isotropic protons, cf. Figure 3 in Li & Habbal (2000). The magnitude of the maximum growth rate in our case is smaller due to the lower electron temperature and plasma β_e parameters used in our study.

3.2. PFHI: Stimulated by Electrons

In the previous subsection, we have studied the interplay between the PFH and the EFH instabilities in the case when both species are firehose-unstable. As the next step in this subsection, we have varied the electron properties to show their effects on the periodic and aperiodic branches of the PFH instability. The proton temperature anisotropy and corresponding plasma $\beta_{p\|}$ have been fixed, and the electron temperature and temperature anisotropy have been gradually reduced, so that the plasma parameters for the selected cases are as follows:

1. $(T_\perp/T_\|)_p = 0.4$, $\beta_{p\|} = 3.0$, $(T_\perp/T_\|)_e = 0.5$, $\beta_{e\|} = 4.0$
2. $(T_\perp/T_\|)_p = 0.4$, $\beta_{p\|} = 3.0$, $(T_\perp/T_\|)_e = 0.9$, $\beta_{e\|} = 4.0$
3. $(T_\perp/T_\|)_p = 0.4$, $\beta_{p\|} = 3.0$, $(T_\perp/T_\|)_e = 0.9$, $\beta_{e\|} = 2.0$

The first case represents the highly anisotropic hot plasma, studied in the previous subsection, with both electrons and protons being firehose-unstable. Under these conditions, the periodic and aperiodic modes of the PFH instability overlap and mix with the corresponding branches of the EFH instability. The mixing of proton and electron scales is mediated by the FH instabilities, as described above in Section 3.1. In this subsection, we focus our analysis on the PFH instability. We discuss all three parameter sets presented above, including the cases when the electrons are still hot and anisotropic, but their anisotropy is insufficient to drive the EFH instability.

Figure 5 presents a complete picture of the angular and wave-number variations for the wave frequency and growth rates for the PFH instability, at the proton scales for the first case study above, when both species are simultaneously firehose-unstable. The second case of reduced electron temperature anisotropy $(T_\perp/T_\|)_e = 0.9$ is presented in Figure 6, and the third case with reduced electron temperature, implying a reduced $\beta_{e\|} = 2.0$, is described by Figure 7. To properly understand the data analysis, we should keep in mind the model procedure and restrictions applied in our representations. For the angular dependence, we have varied the propagation angle with steps of 5°. To create the dispersion plots and to compute the properties of the plasma for each angle of propagation, we have solved the dispersion relation within a fixed wave-number interval, $k = [0.05, 4]d_i^{-1}$ and have selected the fastest growing (or least damped) mode. Sometimes, there are more than one growing solutions for the same parameter set at a given number of propagations, however, here only the fastest growing solution has been selected. This should be taken into account in the interpretation of all 3D dispersion plots. The color bar shows the increasing level of the growth-rate or wave frequency, and everything below the lowest level (including negative growth rates implying damped modes) remains in white.

Let us discuss in detail the unstable PFH solutions in Figure 5 obtained under a direct influence of anisotropic electrons, and compare them with the PFH solutions obtained in Figures 6 and 7, where this influence is gradually reduced. We can clearly identify the two distinct periodic and aperiodic branches of the PFH instability in these figures. Particularly noticeable in Figure 5 is the maximum growth rate of the APFH branch which extends much beyond the usual proton scales $kd_i = 1$, leading to an immediate conclusion that these growth rates are markedly boosted by the EFH instability, namely, the AEFH branch. This is true for most propagation angles, except for $\theta < 10°$, when both PEFH and AEFH instabilities can be simultaneously present and can both contribute to the enhanced PPFH growth rates (see Figure 1).

Although the selected proton plasma $\beta_\|$ and temperature anisotropy are very similar to the ones used in Hellinger & Matsumoto (2000), due to the anisotropic electrons in our case, the propagating PFH instability extends toward higher propagation angles, e.g., 40° (compare Figure 5 to Plate 4 from Hellinger & Matsumoto 2000). In addition, both the propagating and the non-propagating PFH branches extend toward higher wave-numbers and their growth rates are higher. It is also important to note that for a better visualization of the

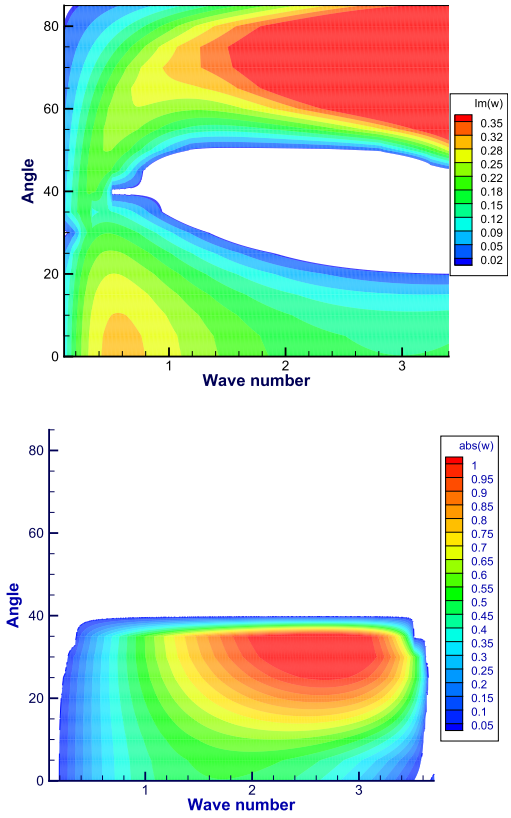

Figure 5. Angular and wave-number dependence of the growth rates (top) and wave frequency (bottom) for the PFH instability. As in Figure 1 the plasma parameters are $(T_\parallel/T_\perp)_p = 0.4$, $(T_\parallel/T_\perp)_e = 0.5$, $\beta_{p\parallel} = 3.0$, $\beta_{e\parallel} = 4.0$. We can distinguish two branches: the periodic branch for parallel propagation and at small angles up to 40°, and the aperiodic modes at highly oblique propagation. A mixing of these two branches becomes apparent at low wave-numbers and for angles less than 40°.

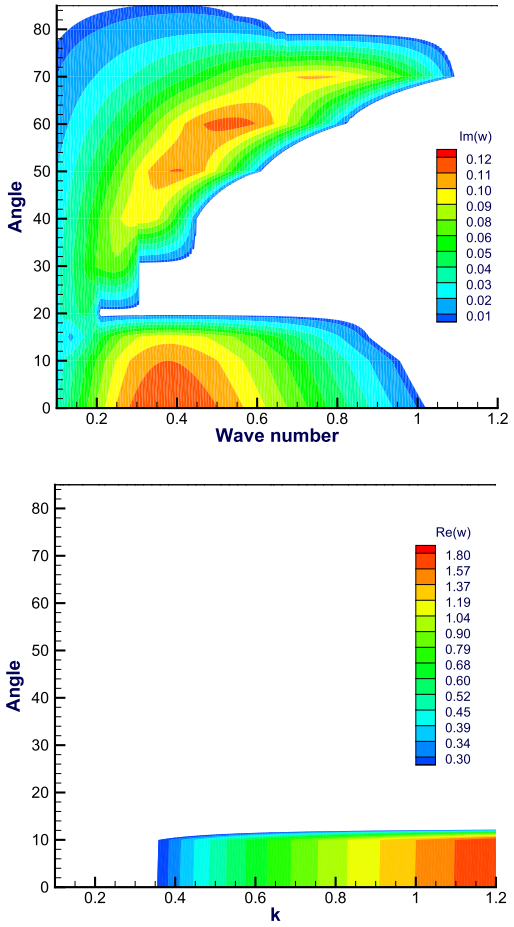

Figure 6. Angular and wave-number dependence of the growth rate (top) and wave frequency (bottom) for the PFH instability when the electron temperature anisotropy is reduced to $(T_\parallel/T_\perp)_e = 0.9$ and all the other parameters are the same. The plot shows the limited range of unstable wave-numbers for the PFH instability, which no longer extends to the electron scales.

growth rate of periodic modes (with peaks much lower than the aperiodic modes) the upper bound of the color-scale has been limited to $\gamma_{\max} \leqslant 0.35\Omega_p$, which represents, in this case, the maximum growth rate for both the quasi-parallel and the oblique PFH instability at scales $kd_i \leqslant 1.5$. However, at higher wave-numbers the maximum growth rate for the extended oblique PFH increases, and, for instance, at $kd_i = 3.5$ it is much higher, $\gamma_{\max} \leqslant 0.84\Omega_p$ (also see Figures 1, 2 and 3). To avoid any numerical uncertainties in the growth rate related to the influence of other dispersion branches, we have plotted the data points with growth rate $\gamma > 0.01\Omega_p$. The observed differences in the linear dispersion originate from the different electron properties and are mainly related to the effect of the electron temperature anisotropy, as became already clear in the analysis from Section 3.1 above.

In order to study the effects of the electron properties on the PFH instability in what follows below, we gradually change the electron temperature anisotropy to have $T_{\perp,e} \approx T_{\parallel,e}$ and decrease the electron temperature. Figure 6 describes the behavior of the PFH instability when a low temperature anisotropy of $(T_\perp/T_\parallel)_e = 0.9$ is considered and all the rest of the plasma parameters are kept unchanged. The new value for the electron temperature anisotropy is insufficient to trigger the EFH instability, therefore only the PFH branches remain. In this case, there is no electron–proton scale mixing and both the periodic and aperiodic PFH branches are confined within the proton scales, i.e., $kd_i < 1.1$. The maximum growth rates of all PFH branches are significantly reduced, being approximately one-third lower than the previous case with highly anisotropic electrons. Similar to the previous cases, at highly oblique angles the PFH instability has an aperiodic nature with zero frequency. The multiple peaks shape of the aperiodic PFH (at large angles) is related to the insufficient resolution in propagation angle, which in this case has been varied each 10°, whereas the resolution in wave-number space is much higher with 1000 points within the entire range of $kd_i = 4$.

Figure 7 shows the wave-number dispersion of the PFH instabilities when the electron temperature and correspondingly, the plasma $\beta_{\parallel e}$, have been reduced by one-half. All the rest of the plasma parameters are kept the same as in Figure 6. Similar to the previous figure, here we have used a reduced angular resolution with a step of 10°. In this case, the aperiodic PFH branch does not extend to very large angles, being fully damped for all wave-lengths above $\theta \geqslant 70°$. On the other hand, the growth of the periodic branch is now restricted to lower angles with $\theta \leqslant 10°$. The maximum growth rates for both the periodic and aperiodic modes are slightly reduced, and the occurrence of these instabilities is further restricted to even lower wave-numbers. The reduced electron temperature leads to a better-resolved separation between the PFH instability branches, namely, the periodic and the aperiodic oblique modes, which are shifted toward lower angles of propagation as

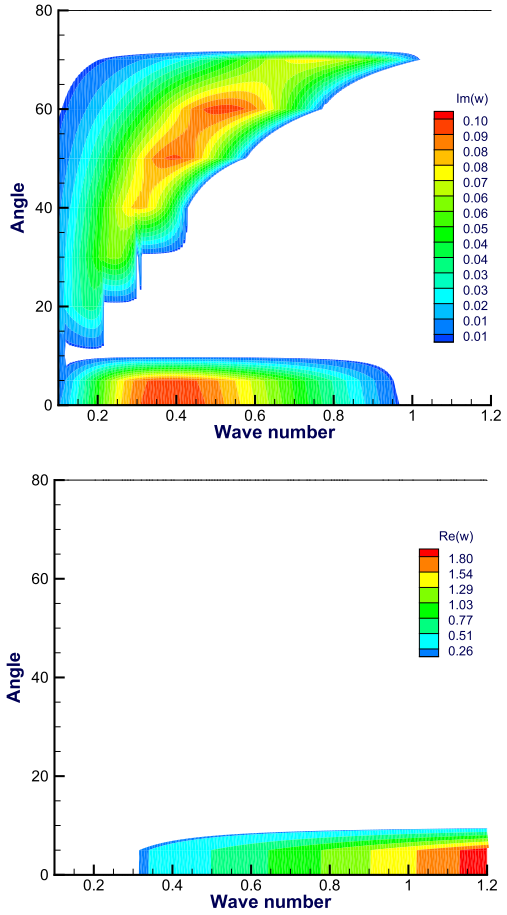

Figure 7. Angular and wave-number dependence of the growth rate (top) and wave frequency (bottom) for the PFH instability when the electron temperature is further reduced such that $\beta_e = 2.0$. The rest of the plasma properties remain unchanged. The plot shows an even more limited range of unstable wave-numbers for the PFH instability.

compared to the previous two cases with hotter and more anisotropic electrons. To conclude, the plots in Figures 5–7 suggestively show a significant influence of the electrons by their thermal spread and temperature anisotropy, on both the periodic and aperiodic branches of the PFH instability.

4. DISCUSSIONS AND CONCLUSIONS

We have solved the general kinetic dispersion relations for firehose-unstable plasmas, using a recently developed linear Vlasov theory IDL solver called PLADAWAN. In this study, we followed the original idea of mixing the proton and electron scales through the excited electromagnetic fluctuations presented for parallel wave propagation by Lazar et al. (2011) and Michno et al. (2014), and elaborated the problem considering the firehose excitations at an arbitrary angle of propagation. In the expanding solar wind, conditions for the FH instabilities are very often satisfied by the plasma particles, mainly electrons and protons, which may exhibit anisotropic velocity distributions due to an excess of parallel temperature or field-aligned beams. This work unifies the conditions of PFH and EFH instabilities, by considering both the electrons and protons anisotropic with $T_{\parallel} > T_{\perp}$ and without any additional beams. Previously, these instabilities were extensively studied but independently of each other by Hellinger & Matsumoto (2000), Li & Habbal (2000) and Camporeale & Burgess (2008).

Section 3.1 describes in detail the interplay of these two instabilities for a representative case of simultaneously anisotropic electrons and protons. Their full wave-vector spectrum has been analyzed, covering the proton and electron scales and the oblique angles of propagation. The main concluding remarks can be iterated here as follows: (1) the interplay of the PFH and EFH instabilities is first revealed by their periodic branches at low wave-numbers (proton scales) and relative low angles of propagation $\theta < 10°$: the periodic PFH (PPFH) is overlapping with the periodic EFH (PEFH) in the wave-number regimes where the electromagnetic field changes from RH to LH polarization. Both of the PPFH and PEFH instabilities operate at the ion scales and their peaks are separated by a few inverse proton inertial lengths. This behavior of the propagating EFH instability might have important implications for ion heating and inverse energy transfer from the small electron to the larger proton scales. These instabilities exhibit growth rates in quasi-parallel direction. (2) As we increase the angle of propagation the aperiodic growing PFH (APFH) modes quickly start to dominate over the periodic branches, and as we increase the wave-numbers all of these branches become dominated by the AEFH. The APFH extends toward the smaller electron scales, mixing with the AEFH branch. Thus, the APFH and the AEFH instabilities co-exist at the intermediate scales with $kd_i > 1$. Both aperiodic modes have the same linear polarization and the distinction between them is not straightforward. For large angles of propagation, (e.g., $\theta = 70°$), the interplay of these two aperiodic instabilities may give rise to a third intermediary peak, followed by an interval of quasi-stabilized wave-numbers, and then by the highest peak of AEFH instability. (3) In agreement with the distinguishing features found by Camporeale & Burgess (2008), we have not found any aperiodic perturbation in the parallel direction. (4) However, under the mutual effects of electrons and protons, we do find limited wave-number regimes of aperiodic unstable AEFH modes already at very small propagation angles, such as 5° and 10°. For strictly parallel and quasi-parallel propagation with $\theta < 10°$, the PEFH instability has growth rates similar to the PPFH modes, and the two instabilities dominate over the APFH and the AEFH branches. (5) As a rule, with increasing angle of propagation, the maximum growth rate for the AEFH instability shifts toward smaller scales. We have examined the dependence of these instabilities on the angle of propagation and found highest growth rates for both APFH and AEFH instabilities at $\theta \approx 65°$. As expected from the previous EFH studies, the highest growth rates of the AEFH instability are obtained at the electron scales, at $kd_i \approx 22$.

As another remark, we should note that the scale mixing between electrons and protons, induced by the firehose instability, strongly depends on the plasma properties. In Section 3.2, we have focused our analysis on the PFH instability, showing that both PPFH and APFH branches are markedly stimulated by the electrons, especially when the latter exhibit anisotropic temperature with $T_{e,\parallel} > T_{e,\perp}$. The growth rate of the PFH instability increases with increasing electron temperature and electron temperature anisotropy, with predominant temperature in the parallel direction. As the electrons become more isotropic they are no longer EFH unstable. Therefore, the scales between the two plasma species decouple

and the PFH instability is restricted to occur at larger scales with wavelengths within the proton inertial length. As we additionally decrease the electron temperature, the growth rate of the PFH instability is further reduced. Independent of the electron properties, though, the PFH always exhibit the two distinct branches with propagating modes at low angles and non-propagating (aperiodic) modes at larger angles. The same remains true for the EFH instability (see the results in Section 3.1).

To conclude, we have shown new theoretical proofs that for the considered temperature and temperature anisotropy conditions, which may be encountered in the solar wind and planetary magnetospheres, the electrons and the protons can interact and exchange energy via the resulting firehose instabilities. These instabilities generate fast aperiodic fluctuations over a broad range of wave-numbers, starting at the protons scales and extending up to the lower electron scales. The maximum growth rate of the AEFH instability occurs at the electron scales, but as we decrease the angle of propagation the peak shifts back toward larger scales and its growth rate gets significantly reduced. However, the AEFH branches remain faster than the APFH at the larger proton (ion) scales, therefore, the anisotropic electron properties cannot be neglected when studying plasma instabilities at the ion scales. At the proton scales the EFH and PFH compete with each other in most cases with comparable growth rates until $kd_i = 3.5$, where the EFH instability grows faster and dominates over the PFH one. Yet, the unstable branches generated by the EFH instability extend down to the ions scales and co-exist with the PFH branches, thus providing a channel for energy transfer between the electrons and protons practically at all angles of propagation. In such a way, for example, some of the electron heat flux energy hidden in the strahl, which results in an overall firehose-unstable configuration of the electron distribution functions, might be relaxed via the EFH instability, and could provide energy for consequent ion scattering. Analogously, the unstable proton distributions can be relaxed by generating propagating or aperiodic structures at lower scales. To properly study these subsequent mechanisms and the related particle scattering and wave-particles interactions, one has to perform direct numerical analysis of the quasilinear and nonlinear evolution of the PFH and EFH instabilities, based on kinetic models such as multi-species PIC or Vlasov simulations, but these tasks will be the objective of our next investigations.

For further information on PLAWADAN and to obtain the source code contact directly A.F. Viñas. This work was supported by project grant C 90347 (ESA Prodex 9) and FWO 12K1416N postdoctoral fellowship at CmPA, KU Leuven. We are grateful to P. Moya for various discussions and fruitful suggestions regarding the dispersion analysis. We thank A. Van Marle for his invaluable hints in visualization techniques. M. Lazar acknowledges funding from the Alexander von Humboldt Foundation during a three-month fellowship at the Ruhr-University Bochum. This work was partially co-funded by projects GOA/2015-014 (KU Leuven), G0A2316N (FWO-Vlaanderen) and the Inter-university Attraction Poles Programme initiated by the Belgian Science Policy Office (IAP P7/08 CHARM). A. F. Viñas wishes to acknowledge the Wind/SWE project for the support of this work.

REFERENCES

Bale, S. D., Kasper, J. C., Howes, G. G., et al. 2009, PhRvL, 103, 211101
Baumjohann, W., & Treumann, R. A. 1996, Basic space plasma physics (London: Imperial College Press)
Bruno, R., & Carbone, V. 2013, LRSP, 10, 2
Camporeale, E., & Burgess, D. 2008, JGR, 113, A07107
Fried, B. D., & Conte, S. D. 1961, The Plasma Dispersion Function (New York: Academic)
Gary, S. P., & Nishimura, K. 2003, PhPl, 10, 3571
Hellinger, P., & Matsumoto, H. 2000, JGR, 105, 10519
Hellinger, P., Trávníček, P., Kasper, J. C., & Lazarus, A. J. 2006, GeoRL, 33, L09101
Hellinger, P., Trávníček, P. M., Decyk, V. K., & Schriver, D. 2014, JGRA, 119, 59
Ichimaru, S. 1973, in Basic Principles of Plasma Physics, a Statistical Approach, ed. S. Ichimaru (Reading, MA: Benjamin), 324
Jian, L. K., Russell, C. T., Luhmann, J. G., et al. 2009, ApJL, 701, L105
Kasper, J. C., Maruca, B. A., Stevens, M. L., & Zaslavsky, A. 2013, PhRvL, 110, 091102
Kennel, C. F., & Scarf, F. L. 1968, JGRA, 73, 6149
Krall, N. A., & Trivelpiece, A. W. 1973, Principles of Plasma Physics, International Student Edition—International Series in Pure and Applied Physics (Tokyo: McGraw-Hill Kogakusha)
Lazar, M., & Poedts, S. 2009, A&A, 494, 311
Lazar, M., Poedts, S., & Schlickeiser, R. 2011, A&A, 534, A116
Li, X., & Habbal, S. R. 2000, JGR, 105, 27377
Maneva, Y. G., Ofman, L., & Viñas, A. 2015, A&A, 578, A85
Maneva, Y. G., Viñas, A. F., Moya, P. S., Wicks, R. T., & Poedts, S. 2015, ApJ, 814, 33
Messmer, P. 2002, A&A, 382, 301
Michno, M. J., Lazar, M., Yoon, P. H., & Schlickeiser, R. 2014, ApJ, 781, 49
Montgomery, D. C., & Tidman, D. A. 1964, Plasma Kinetic Theory (New York: McGraw-Hill)
Navarro, R. E., Moya, P. S., Muñoz, V., et al. 2014, PhRvL, 112, 245001
Nguyen, S. T., Perez, J. D., & Fennell, J. F. 2007, JGR, 112, A12203
Paesold, G., & Benz, A. O. 1999, A&A, 351, 741
Shaaban, M. S., Lazar, M., Poedts, S., & Elhanbaly, A. 2015, ApJ, 814, 34
Stix, T. H. 1962, The Theory of Plasma Waves (New York: McGraw-Hill)
Viñas, A. F., Moya, P. S., Navarro, R. E., et al. 2015, JGRA, 120, 3307
Viñas, A. F., Wong, H. K., & Klimas, A. J. 2000, ApJ, 528, 509–23
Yoon, P. H., & Seough, J. 2014, JGRA, 119, 7108
Zimbardo, G., Greco, A., Sorriso-Valvo, L., et al. 2010, SSRv, 156, 89